ELSEVIER

Journal of Nuclear Materials 264 (1999) 271–282

journal of nuclear materials

Temperature programmed decomposition of uranyl nitrate hexahydrate

S. Dash [a], M. Kamruddin [a], Santanu Bera [b], P.K. Ajikumar [a], A.K. Tyagi [a], S.V. Narasimhan [b], Baldev Raj [a,*]

[a] *Metallurgy and Materials Group, Indira Gandhi Centre for Atomic Research, Kalpakkam 603 102, Tamil Nadu, India*
[b] *Water and Steam Chemistry Laboratory, BARC Facilities, Kalpakkam 603 102, Tamil Nadu, India*

Received 17 April 1997; accepted 5 August 1998

Abstract

Temperature programmed decomposition (TPD) of uranyl nitrate hexahydrate has been studied using evolved gas analysis mass spectrometry (EGA-MS) in the temperature range 300–1400 K. Thermogravimetric (TGA) investigations were performed in the temperature range 300–1100 K. An attempt has been made to resolve the complexity of decomposition behaviour through suitable comparison of TGA and EGA-MS data. Kinetic control regimes for various decomposition stages could be deduced from EGA-MS data. The corresponding activation energies and frequency factors were also evaluated. Kinetics based on random nucleation and diffusion was found to be rate controlling. The residue left over after each decomposition stage was analysed by XRD and XPS to determine structure and composition. The ultimate product was found to be a mixture of $UO_3H_{1.17}$ and U_3O_8: the former being a topotactic hydrogen spill over compound of UO_3. Complete conversion of this residue to U_3O_8 was noticed during ion beam exposure of the residue which was performed in the course of XPS investigations.

PACS: 82.30.Lp; 07.75.+h; 82.30.Pm; 82.80.Pv

1. Introduction

Product consolidation constitutes an essential step in the reprocessing of nuclear fuel cycle [1–3]. Both thermal as well as microwave induced denitration of nitrate salt solutions are often preferred due to several advantages [4,5]. Through this route, nuclear reactor ceramic fuel materials like UO_2 and PuO_2 can be prepared with excellent powder characteristics. Mixed oxides like $(U,Th)O_{2+x}$, $(U,Pu)O_{2\pm x}$ can be prepared through co-denitration of respective nitrate salt solution followed by high temperature calcination [6]. In this processing route, hydrates of $UO_2(NO_3)_2$, $Th(NO_3)_4$ and $Pu(NO_3)_4$ are encountered as important precursors. In this context, thermal stability and proper solid state decomposition kinetic studies along with mapping of mechanistic pathways assume significance for optimising applicator design [7]. For this reason, the compound uranyl nitrate hexahydrate has, in particular, been the focus of various experimental investigations. These studies were directed at deriving structural information through X-ray diffraction (XRD) [8], neutron diffraction [9] and infrared spectroscopy measurements [10]. Along with uranyl nitrate hexahydrate, other derivative compounds like uranyl nitrate dihydrate, α, β and γ-$UO_2(OH)_2$, UO_3, U_3O_8, $UO_3 \cdot xH_2O$ besides several polynuclear uranyl complexes formed during hydrolysis as well as melting [11] have been investigated.

Ondrejcin et al. [12] working on the decomposition of $UO_2(NO_3)_2 \cdot 2H_2O$ in vacuum and in air have concluded a sequential dehydration of $UO_2(NO_3)_2 \cdot 2H_2O$ leading to formation of polymorphous UO_3 and its hydrates through $UO_2(OH)NO_3$ as an important intermediate. Lodding et al. [13] have studied thermal decomposition of uranyl nitrates in presence of steam. They have reported sequential dehydration followed by

* Corresponding author.

0022-3115/99/$ – see front matter
PII: S0022-3115(98)00495-4

decomposition to $UO_3(.8H_2O)$. Woodhead et al. [11] have observed evolution of polynuclear uranyl hydroxy nitrate complexes during hydrolysis and melting of $UO_2(NO_3)_2 \cdot xH_2O$ at 70°C. Formation of several hydrolysed and polymerised products during thermal decomposition of uranyl nitrate hexahydrate has also been reported by Rajagopalan et al. [14]. Franklin et al. [15] have studied dehydration kinetics of uranyl nitrate hexahydrate single crystals under vacuum. They have observed sequential transformation of

$$UO_2(NO_3)_2 \cdot 6H_2O \rightarrow UO_2(NO_3)_2 \cdot 3H_2O \rightarrow UO_2(NO_3)_2 \cdot 2H_2O \rightarrow UO_2(NO_3)_2 \cdot H_2O \rightarrow UO_2(NO_3)_2.$$

The authors observed prevalence of contracting envelope kinetics and linear dependence of dehydration on water vapour pressure. Similar sequential multistep dehydration of $UO_2(NO_3)_2 \cdot 6H_2O$ has also been reported by Smith [16]. In their study of isothermal dehydration of uranyl nitrate hexahydrate, Moseley et al. [17] observed catalytic activity of product gases leading to lowering of conversion activation energies. Contraries to above studies, Weigel et al. [18] have indicated nonviability of preparing anhydrous uranyl nitrate from uranyl nitrate hexahydrate by thermal decomposition.

In the backdrop of above, the authors noticed the following: (1) complex multistep weight loss profiles observed in TGA have not been explained (2) evaluation of product stoichiometry in terms of oxygen to metal ratio needs to be established and (3) thermo kinetic investigation on decomposition of $UO_2(NO_3)_2 \cdot 6H_2O$ at temperatures beyond 1000 K has not been reported. To address these points we have investigated the temperature programmed decomposition of $UO_2(NO_3)_2 \cdot 6H_2O$ (UNH) using evolved gas analysis by mass spectrometry (EGA-MS), thermogravimetric analysis (TGA), X-ray diffraction (XRD) and X-ray photoelectron spectroscopy (XPS). The EGA technique based on mass spectrometry has significant advantages in terms of sensitivity, specificity, fast response and multi-channel detection capability [19–21]. The present study was performed in dynamic high vacuum environment as the mechanistic pathway followed by decomposition is critically dependent on sample environment. Vacuum ensures perfect non-equilibrium situation by way of fast pumping of released gases, which may otherwise lead to recombination/inhibition effects [22]. Besides explaining complex weight loss behaviour seen in TGA, the EGA-MS data was used to derive the fractional extent of reaction 'α' and to deduce functional transform '$f(\alpha)$' of non-isothermal solid state kinetic rate expressions [23,24]. This was used to assess the corresponding integral model function $g(\alpha)$ [25–27]. Various stages of decomposition were found to comply with models based on random nucleation and diffusion [28]. The off-line characterisation of residues left over after each decomposition stage, marked by distinct oxygen release regimes, was carried out by powder XRD and XPS for studying structural and compositional variations resulting from temperature programme. This was done to elucidate the mechanistic pathway leading to the formation of U_3O_8.

2. Experimental

$UO_2(NO_3)_2 \cdot 6H_2O$ powder sample procured from M/s BDH Chemicals, USA, was used for temperature programmed decomposition in the EGA-MS facility. Typical sample weights of 100 mg and particle size of 50 μ were subjected to a maximum temperature of 1400 K at heating rates of 4, 6 and 10 K/min. The details of the EGA-MS facility have been published elsewhere [29,30] and only a brief description will be furnished here. A line schematic of the system is given in Fig. 1. Essentially, this facility consist of a high temperature (1400 K), high vacuum (10^{-7} mbar), programmable resistance furnace coupled to an ultra high vacuum (UHV) chamber (10^{-11} mbar) through a low conductance variable aperture molecular leak valve. The UHV chamber houses quadrupole mass spectrometer (QMS), vacuum gauges and other metrological calibration hardware like spinning rotor gauge (SRG) and standard gas inlets. The high vacuum chamber is pumped by a turbomolecular

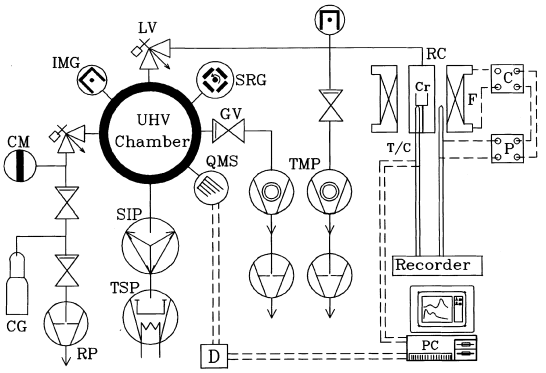

TMP–Turbo Molecular Pump
IMG–Inverted Magnetron Gauge
QMS–Mass Spectrometer
SIP–Sputter Ion Pump
SRG–Spinning Rotor Gauge
CG–Calibration Gas
CM–Capacitance Manometer
P–PID Temp. Programmer
TSP–Ti Sublimation Pump
RP–Rotary Pump
LV–Leak Valve
GV–Gate Valve
C–Power Controller
T/C–Thermocouple
RC–Reaction Chamber
Cr–Crucible
F–Resistance Furnace
D–QMS Controller

Fig. 1. Line schematic of experimental EGA-MS facility.

pumping system. A pumping group consisting of a triode sputter ion pump, a titanium sublimation pump and a separate turbomolecular pumping system evacuates the UHV chamber. A PC based software developed by us executes real time Multiple Ion Detection (MID) mass spectrometry. TPD profiles are obtained by plotting MID signals against the sample temperature measured by a calibrated K-type thermocouple and acquired through a PC based add-on card.

TGA runs for UNH were conducted in a Polymerlab, UK make PL STA 1500 thermal analyser under an argon carrier gas flow of 40 ml/min. Due to certain limitations, the TGA data was acquired in the temperature range 300–1100 K. For the purpose of comparison, TGA curve was superimposed over EGA curve for similar heating rate. Since sample environments in TGA and EGA are different minor discrepancy in temperature was noticed.

XRD and XPS investigations were carried out on residues of samples heated at 10 K/min. The residues were withdrawn after each decomposition stage by interrupting the temperature programme at 790, 950 and 1400 K termed as stage I, stage II and stage III, respectively. XRD analyses were performed using a Siemen's D-5000 X-ray diffractometer. XPS measurements were carried out with a VG ESCALAB MK200X ESCA machine using aluminium K_α X-ray source (1486.6 eV) and a hemispherical analyser which was operated on a pass energy of 20 eV giving analyser resolution of 0.4 eV. Photoelectron emission spectra of U($4f_{7/2}$), O(1s) and C(1s) were recorded with about 0.1 eV/point.

3. Results and discussion

3.1. Kinetic analysis

The rate of a temperature programmed decomposition reaction is expressed as

$$r = \mathrm{d}\alpha/\mathrm{d}t = k(T) * f(\alpha), \tag{1}$$

where α is fractional extent of decomposition directly measurable from gas release data. This is defined as

$$\alpha(T) = Q(T)/Q(\mathrm{Total}) = A(T)/A(\mathrm{Total}),$$

where $Q(T)$ and $Q(\mathrm{Total})$ pertain to instantaneous and total gas corresponding to area under the release curves $A(T)$ and $A(\mathrm{Total})$ respectively. Measurement of experimental $\alpha(T)$ is further illustrated in Fig. 2(a) and (b). $f(\alpha)$ represents a functional transform of α as an indicator of instantaneous phase composition at a given temperature [31]. This functional transform $f(\alpha)$ expressible as analytical functions is critically dependent on kinetic control mechanisms like random nucleation,

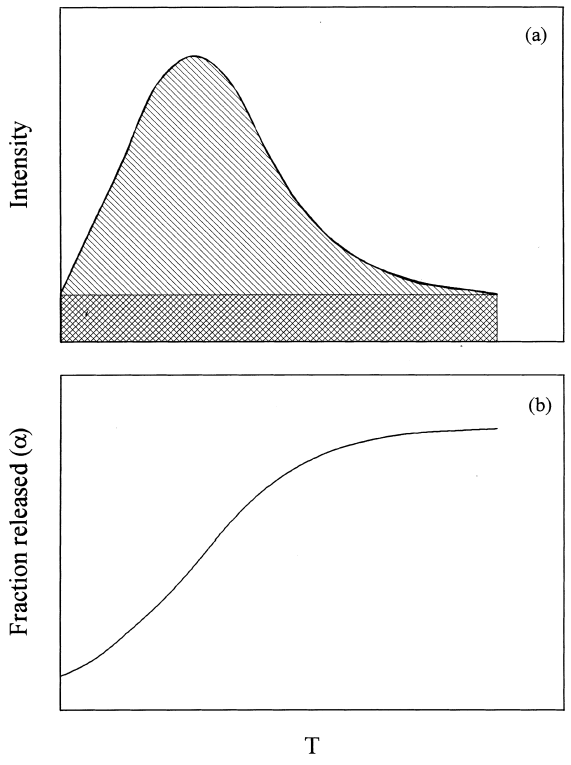

Fig. 2. Calculation of fractional reaction parameter 'α': (a) model trend analysis mass spectrum and (b) fractional reaction plot.

diffusion and phase boundary interface motion [32]. A list of such expressions based on above formalisms is given in Table 1. $k(T)$ refers to temperature dependent rate constant having expression

$$k(T) = Z\ \exp(-E/RT), \tag{2}$$

where Z is pre-exponential factor and E is activation energy barrier. TPD experiment allows us to evaluate $k(T)$ and $f(\alpha)$. For a linear temperature schedule $T = T_\mathrm{o} + \beta t$, where β stands for heating rate, the expression assumes the form

$$\mathrm{d}\alpha/\mathrm{d}T = Z/\beta(\exp(-E/RT)) * f(\alpha). \tag{3}$$

The integration of above expression within limit yields

$$g(\alpha) = \int_0^\alpha \mathrm{d}\alpha/f(\alpha) = Z/\beta \int_0^T \exp(-E/RT)\mathrm{d}T \tag{4}$$

with necessary series solution and suitable approximations the integral reduces to

$$g(\alpha) = ZRT^2/\beta E * \exp(-E/RT). \tag{5}$$

In logarithmic form this yields

$$\ln[g(\alpha)/T^2] = \ln(ZR/\beta E) - E/RT. \tag{6}$$

Table 1
Non isothermal, integral forms of kinetic expression for heterogeneous solid-state reactions

Rate determining mechanism	Symbol	$f(\alpha)$	$g(\alpha) = \int_0^{\infty} d(\alpha)/f(\alpha)$
Nucleation and growth models			
(i) Random nucleation approach			
Mampel unimolecular law	A1	$1-\alpha$	$-\ln(1-\alpha)$
(ii)Avrami–Erofeev nuclei growth			
(a) 2-dimensional growth	A2	$2(1-\alpha)[-\ln(1-\alpha)]^{1/2}$	$[-\ln(1-\alpha)]^{1/2}$
(b) 3-dimensional growth	A3	$3(1-\alpha)[-\ln(1-\alpha)]^{2/3}$	$[-\ln(1-\alpha)]^{1/3}$
(iii) Branching nuclei			
Prout Tompkins branching nuclei	A4	$\alpha(1-\alpha)$	$\ln[\alpha/(1-\alpha)]$
Decelerating rate equations based on diffusion			
(i) Parabolic law			
1-dimensional transport	D1	α^{-1}	$\alpha^2/2$
(ii) 2-dimensional diffusion	D2	$[-\ln(1-\alpha)]^{-1}$	$(1-\alpha)[\ln(1-\alpha)]+\alpha$
(iii) 3-dimensional diffusion (Jander–Mech)	D3	$(1-\alpha)^{1/3}[(1-\alpha)^{-1/3}-1]^{-1}$	$1.5[1-(1-\alpha)^{1/3}]^2$
(iv) 3-dimensional diffusion (Ginstling–Brounshtein)	D4	$[(1-\alpha)^{-1/3}-1]^{-1}$	$1.5[1-2\alpha/3-(1-\alpha)^{2/3}]$
Phase boundary movement			
(i) 1-dimensional (Zero order)	R1	Constant	α
(ii) 2-dimensional (cylindrical symmetry)	R2	$(1-\alpha)^{1/2}$	$2[1-(1-\alpha)^{1/2}]$
(iii) 3-dimensional (spherical symmetry)	R3	$(1-\alpha)^{2/3}$	$3[1-(1-\alpha)^{1/3}]$

The $g(\alpha)$ denotes the integral form of non-isothermal rate expressions. These expressions are given alongside $f(\alpha)$ in Table 1.

A plot of $\ln[g(\alpha)/T^2]$ vs. $1/T$ yields a straight line whose intercept and slope give $\ln(ZR/\beta E)$ and $(-E/R)$ respectively. In our procedure we have computed $\ln[g(\alpha)/T^2]$ from the measured α versus T values and fitted it against theoretical $g(\alpha)$ expressions propounded for various kinetics control models. The best fit has been regarded as prevailing mechanism and it is utilised for evaluation of activation energy E and pre-exponential factor Z [33]. A typical case is illustrated in Fig. 3 which shows governance of random nucleation based Mampel unimolecular law on dehydration kinetics of $UO_2(NO_3)_2 \cdot 6H_2O$.

3.2. EGA-MS studies

Fig. 4(a), Fig. 5(a) and Fig. 6(a) depict TPD spectra of $UO_2(NO_3)_2 \cdot 6H_2O$ acquired at heating rates of 4, 6 and 10 K/min, respectively. The corresponding fraction release plots are shown in Figs. 4(b), 5(b) and 6(b), respectively. Release of various gaseous species like H_2O ($m/e = 18$), NO ($m/e = 30$), O_2 ($m/e = 32$) and NO_2 ($m/e = 46$) have been recorded as a function of time and temperature. The dehydration of the sample, in air as well as in vacuum takes place in the temperature range 300–525 K. The final dehydration profile appears to be bimodal. The decomposition reaction leading to evolution of NO, NO_2 and O_2 commences around 420 K which is below the completion temperature of dehydration. The corresponding fractional release plots show two NO release stages, one O_2 release stage and one NO_2 release stage. The decomposition is followed by a second O_2 release stage peaked at around 810 K. At higher heating rates i.e. at 6 and 10 K/min, an additional O_2 release stage peaked at 1300 K appears (Figs. 5(a) and 6(a)).

The kinetics evaluation procedure, as explained earlier was adopted to establish kinetic control regimes for different dehydration and decomposition stages and to determine associated arrhenius parameters like activation energy and the pre-exponential factors. The dehydration stage observed in EGA was found to be

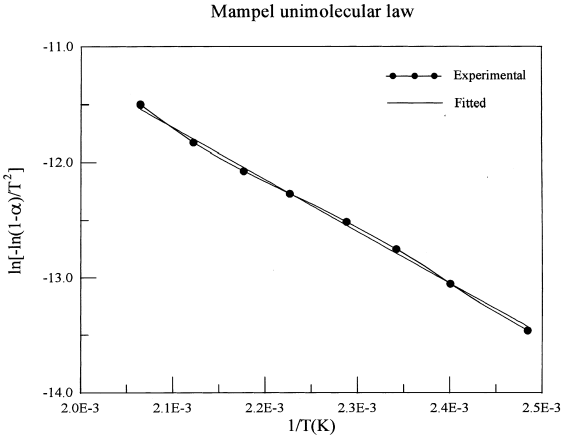

Fig. 3. Typical non-isothermal kinetic analytical fit showing prevalence of Mampel unimolecular law in dehydration stage.

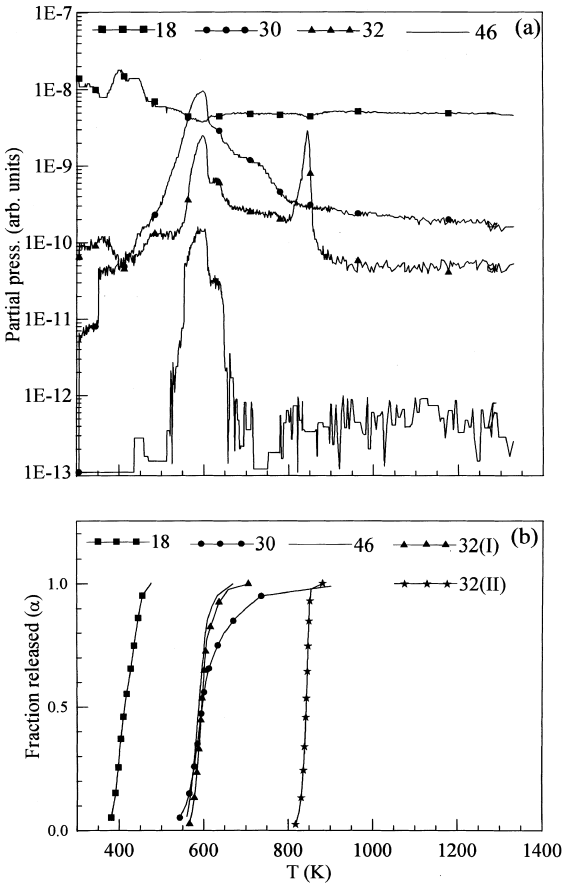

Fig. 4. (a) EGA-MS plot for temperature programmed decomposition of $UO_2(NO_3)_2 \cdot 6H_2O$ at heating rate of 4 K/min and (b) the corresponding fraction release plot.

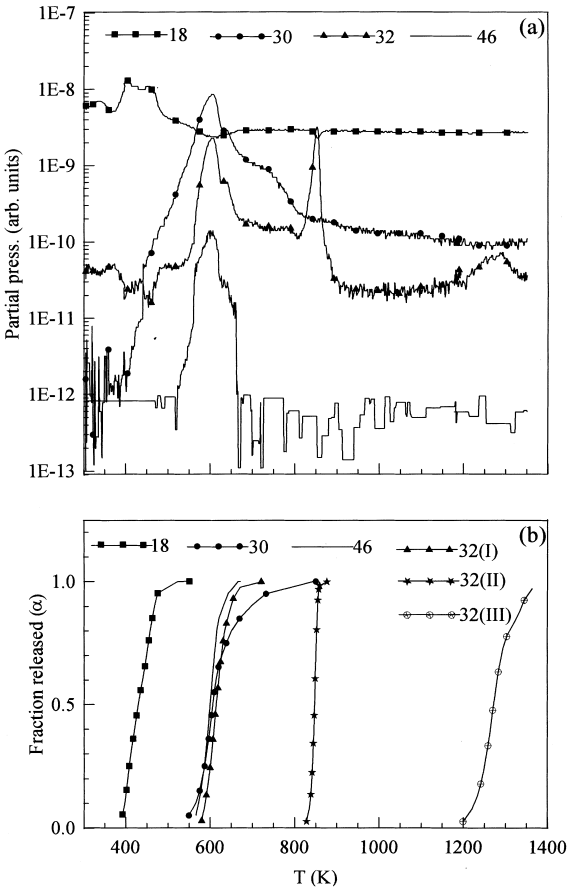

Fig. 5. (a) EGA-MS plot for temperature programmed decomposition of $UO_2(NO_3)_2 \cdot 6H_2O$ at heating rate of 6 K/min and (b) the corresponding fraction release plot.

controlled by random nucleation. The multimodal dehydration observed in TGA and EGA-MS occurs due to sequential multistep desorption of crystallographically non-equivalent highly labile structural water molecules. In uranyl nitrate hexahydrate, the oxygen atoms of two water molecules along with four others from two bidentate nitrate groups are co-ordinated directly to the central metal cation making a planar equatorial hexagon around uranyl group. These two directly co-ordinated water molecules are distinctly different from hydrogen bonded structural water and give rise to well defined EGA-MS signal. A part of this water is probably carried forward beyond this dehydration stage. However, owing to overlapping NO_x release, the stoichiometry conjectured to be $UO_2(NO_3)_2 \cdot 2H_2O$ could not be examined off-line. The subsequent TGA investigations have substantiated this. Barring structural water, the basic co-ordination of uranium in $UO_2(NO_3)_2 \cdot 2H_2O$ is identical with that of $UO_2(NO_3)_2 \cdot 6H_2O$ [34]. No change in this rate governing mechanism was observed with increase in heating rate. The values of activation energy and pre-exponential factor were determined and are given in Table 2.

The dehydration regime as stated above partially overlaps with initial decomposition stage signalled by release of NO, NO_2 and O_2. Surface dominated kinetics control i.e. random nucleation behaviour manifests in this regime also. However, second stage NO release shows governance by three-dimensional diffusion mechanism propounded through Jander–Mech rate expression. The reason can be attributed to product barrier layer formation, a phenomena commonly seen in many technical gas–solid reactions [35]. The origin of two stage temperature dependant NO_x release can be traced to two distinct categories of formula molecular units in monoclinic lattice of $UO_2(NO_3)_2 \cdot 2H_2O$. One N–O uncoordinated bond derives additional stability due to hydrogen bonding. This has also been confirmed from reduced thermal motion of N–O oxygen atom [36].

After the completion of gross decomposition a second oxygen release peak appears. The kinetics was once again found to be random nucleation controlled. The

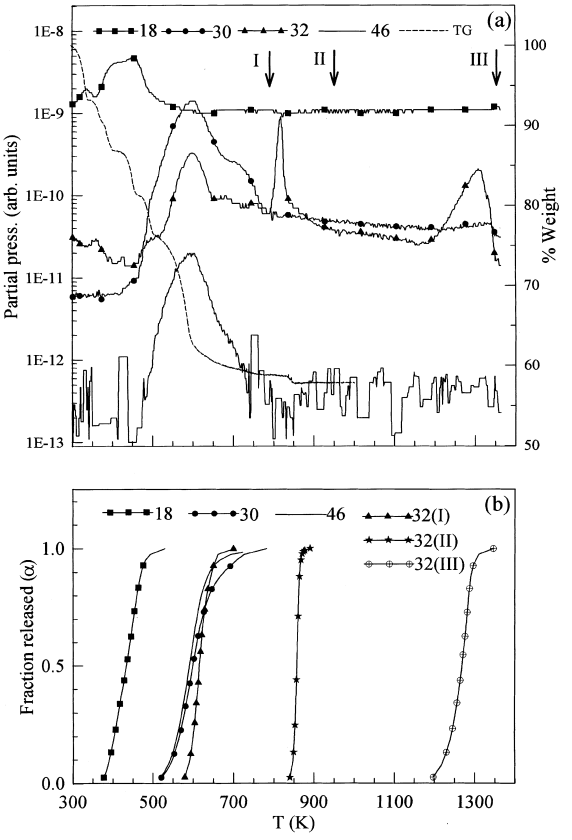

Fig. 6. (a) EGA-MS plot for temperature programmed decomposition of $UO_2(NO_3)_2 \cdot 6H_2O$ superimposed on TGA weight loss curve at heating rate of 10 K/min and (b) the corresponding fraction release plot.

reason can be attributed to uncovering of freshly exposed lattice sites having oxygen-bearing groups [37]. The corresponding activation energy and pre-exponential factors were derived and are given in Table 2.

At higher heating rates of 6 and 10 K/min, a third oxygen release peak appears in the temperature range 1180–1360 K. At this point, thermal gradient driven mass transfer effects become significant [38,39]. This leads to migration and release of lattice oxygen resulting in the loss of stoichiometry. The analogy of this phenomena exists in operating nuclear fuel elements at high temperature gradients [40]. As in stage II oxygen release, here also the kinetic control shows governance by random nucleation [28]. The corresponding activation energy and pre-exponential factor are given in Table 2.

3.3. TGA investigations

Complex TGA weight loss profile was super imposed on EGA data acquired for 10 K/min (Fig. 6(a)). The complex TGA weight loss profile was deconvoluted to reveal seven sub-stages corresponding to decomposition in the temperature range 300–750 K. These sub-stages are termed as IA, IB, IC, ID, IE, IF and IG (Fig. 7). The 8th stage at 840 K coincides with stage II oxygen release stage in EGA-MS spectra. The first three weight loss stages, before 400 K, corresponds to loss of two water molecules, one water molecule and one water molecule respectively. The corresponding portion of EGA-MS spectra shows a small water release step. Most of these water molecules are highly labile structural water and gets released during vacuum operation. It was observed from weight loss that the sample looses four molecules of water while in vacuum but regains it back upon exposure to atmosphere. Stage ID weight loss (5.35%) occurs in the temperature range 420–460 K and accounts for release of roughly $1\frac{1}{2}$ molecules of water. Stage IE weight loss overlaps with onset of decomposition. The weight loss of 5.01% can be accounted for through release of $\frac{1}{2}$ moles of NO_2 and O_2. Since no significant water signal observed in this temperature range, it is presumed that remaining water molecules were carried forward. The stage IF weight loss occurs in the temperature range 520–600 K and amounts to 14.6%. This can be accounted for through release of NO_2 and $\frac{1}{2}$ O_2. Stage IG weight loss spreads over 600–750 K is a gradual one amounting to 2.63%. This can be accounted for through decomposition of residual nitrate. The 8th stage weight loss of 1.2% can be attributed to O_2 release signal. However, in TGA it spans over 835–850 K compared to EGA span 800–850 K. The marginal deviation results from different sample environments seen in TGA and EGA. Due to operational limitations of TGA machine the temperature regime could not be extended beyond 1100 K. Hence the high temperature O_2 release stage observed in EGA over 1180–1360 K is not seen.

3.4. XRD Studies

The effect of temperature programme on substrate crystal structure was investigated by X-ray powder diffraction. In addition to raw sample, residues withdrawn after various oxygen release stages (Fig. 4(a)) were also analysed. The XRD pattern of raw sample, stage I, stage II, and stage III residues are shown in Fig. 8(a)–(d) respectively. The raw $UO_2(NO_3)_2 \cdot 6H_2O$ sample, as reported [8,9], consisted of an orthorhombic non-centre symmetric layered lattice. In this compound each formula unit consists of an uranyl group surrounded equatorially by a near planar oxygen hexagon of four oxygen atoms from two non-equivalent bidentate nitrate groups and two oxygen atoms from equivalent water ligands. All the hydrogen atoms are involved in hydrogen bonding. Four structural water molecules are outside the primary co-ordination sphere. The formula can be expressed as $[UO_2(H_2O)_2(NO_3)_2] \cdot 4H_2O$. These four structural water molecules outside the co-ordination

Table 2
Reaction mechanism, corresponding correlation coefficients, activation energy and pre-exponential factors for various stages of decomposition of $UO_2(NO_3)_2 \cdot 6H_2O$ at different heating rates

Heating rate (K/min)	Mechanism	Correlation coefficient	Activation energy (kJ/mol)	Pre-exponential factors (m^{-1})
Dehydration: stage I				
4	A1	0.9942	87.011	1.99×10^{10}
6	A1	0.9897	56.414	1.53×10^{6}
10	A1	0.9934	53.828	8.17×10^{5}
Dehydration: stage II				
4	A1	0.9951	43.971	2.98×10^{4}
6	A1	0.9923	42.724	2.0×10^{4}
10	A1	0.9992	47.268	1.02×10^{5}
NO release: stage I				
4	A1	0.9991	120.56	4.1×10^{9}
6	A1	0.9998	123.33	7.2×10^{9}
10	A1	0.9982	82.413	2.9×10^{6}
NO release: stage II				
4	D3	0.9860	33.078	4.2
6	D3	0.9710	41.522	34.5
10	D3	0.9969	33.778	15.3
NO_2 release				
4	A1	0.9940	176.84	7.9×10^{14}
6	A1	0.9999	134.52	1.2×10^{11}
10	A1	0.9959	84.297	5.5×10^{6}
O_2 release: stage I				
4	A1	0.9970	212.38	8.1×10^{17}
6	A1	0.9950	160.85	9.7×10^{12}
10	A1	0.9967	145.28	1.8×10^{12}
O_2 release: stage II				
4	A1	0.9994	962.88	2.4×10^{59}
6	A1	0.9997	1103.89	9.1×10^{67}
10	A1	0.9971	1010.95	6.5×10^{64}
O_2 release: stage III				
6	A1	0.992	458.74	9.2×10^{17}
10	A1	0.9992	560.04	1.0×10^{22}

sphere desorb sequentially in the temperature range 300–400 K owing to loss of exterior hydrogen bonding. Dissociation of UND in air occurs in the temperature range 420–460 K.

Upon completion of dehydration and denitration stages which includes oxygen release stage I, the temperature programme was interrupted at 790 K (after observing NO_x signal falling to background). This residue was subjected to XRD analysis. The compound was revealed to be $UO_3 \cdot xH_2O$. Such partially hydroxylated intermediates have been encountered in other fuel processing routes like decomposition of $(NH_4)_2U_2O_7 \cdot xH_2O$ [41]. $UO_3 \cdot xH_2O$ has been reported as a hydroxylated compound having OH oxygen co-ordinated to uranium atoms. Such co-ordination has been reported by Deane et al. [42] from IR spectroscopic studies. Such hydroxylated compounds where uranium has octahedral co-ordination are known to exist in several interchangeable polymorphic transformations [43–46]. The structure consists of hexagonal or pseudo-hexagonal layers of composition having $UO_2(O_2)_\infty$ chains built in to orthorhombic lattice with water molecules interspersed in between [41].

After stage II oxygen release i.e., beyond 950 K the structure once again transforms to an orthorhombic lattice having molecular formula $UO_3H_{1.17}$. This is a hydrogen insertion compound of UO_3 having almost similar crystallochemical configuration [47]. Such products have also been reported by Lodding et al. [48] as end product of decomposition. Here the structure may be written as $UO_2(OH)_x$ meaning thereby partial hydroxylation of lattice oxygen. $UO_3H_{1.17}$ is topotactic with α-UO_3, which has a layered orthorhombic structure [47]. This structure is construed as uranium deficient

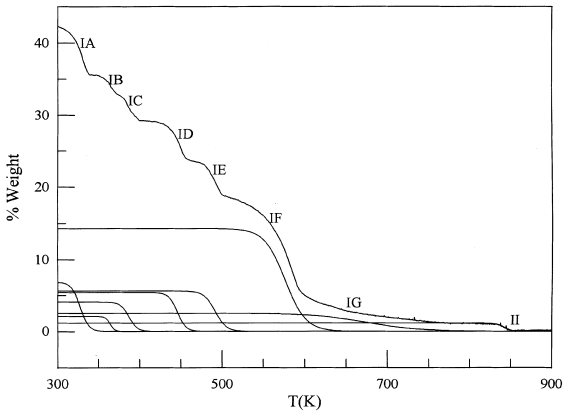

Fig. 7. TGA weight loss curve of $UO_2(NO_3)_2 \cdot 6H_2O$ at 10 K/min deconvoluted to show the eight distinct steps.

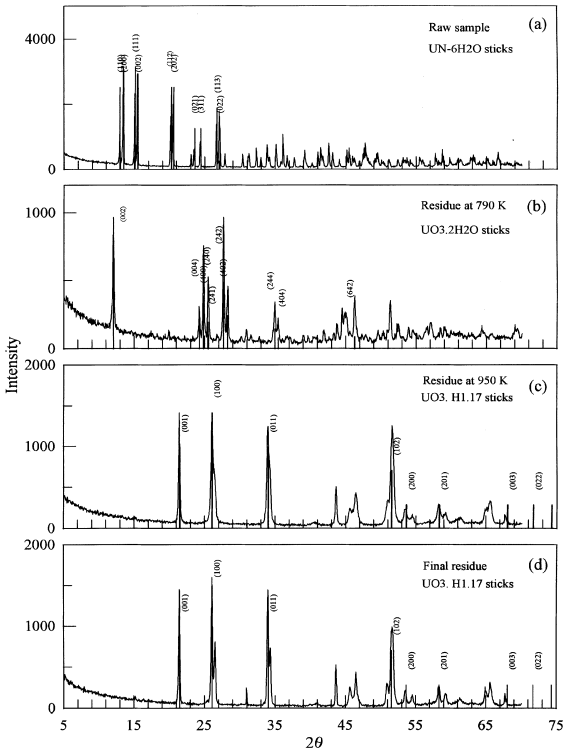

Fig. 8. Powder X-ray diffractograms along with matching JCPDS sticks for: (a) original $UO_2(NO_3)_2 \cdot 6H_2O$ orthorhombic crystal structure; (b) structure of stage I residue after surface dehydration and NO_x release; (c) structure of stage II residue showing onset of formation of $UO_3H_{1.17}$; and (d) well developed structure of the compound $UO_3H_{1.17}$ and U_3O_8 as encountered in stage III residue.

form of α-U_3O_8 consisting of planes of edge sharing pentagonal bipyramids with U–O–U chain running perpendicular to these layers [49]. The spill over hydrogen gets attached to oxygen atoms in a perturbed M–O framework [47] leading to marginal changes in lattice parameter and reduction in symmetry, which results in splitting of diffraction lines. This structure is further developed after stage III oxygen release i.e., beyond 1350 K. Also at this stage indexing of diffraction lines indicated formation of U_3O_8. The stage III residue contains stage II residue along with newly formed U_3O_8. Also a minor carry over from stage I residue still persists. A tentative reaction sequence depicting stoichiometric evolution of various intermediates can be given as follows:

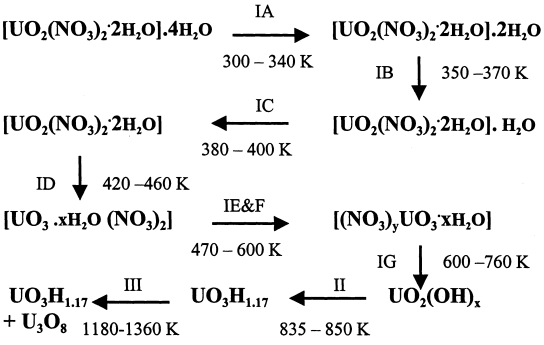

The splitting of diffraction line in final stage compound can also be due to onset of formation of new uranium bearing phase. Some of the diffraction lines matched with reflection pattern from the compound U_3O_8. This signifies partial conversion of $UO_3H_{1.17}$ to U_3O_8. The above scheme has been further corroborated through XPS investigations described in the following section. It can be inferred from XRD studies that the temperature programme resulted in the gradual structural simplification by way of ejection of formula units while retaining the pristine uranyl oxygen bridge.

3.5. XPS studies

Keeping the structural information received from XRD data as background, the chemical environment around uranium was probed by XPS to elucidate the mechanism involved in the conversion of $UO_2(NO_3)_2 \cdot 6H_2O$ to U_3O_8 via various intermediate stages besides mapping of associated alteration in uranium to oxygen ratios. U($4f_{7/2}$) and O(1s) and C(1s) photoelectron peaks were recorded. The binding energy was calibrated with Au($4f_{7/2}$) photoelectron peaks at 84.0 eV with 1.6 eV FWHM for the specimen of Au film on Si substrate. Freshly prepared UO_2 [50] was used as the reference material and O(1s) to U($4f_{7/2}$) photoelectron peak area ratio was observed to be 0.166, is used for reference data to compare the O/U area ratio at the different stages of decomposition(the reference area ratio

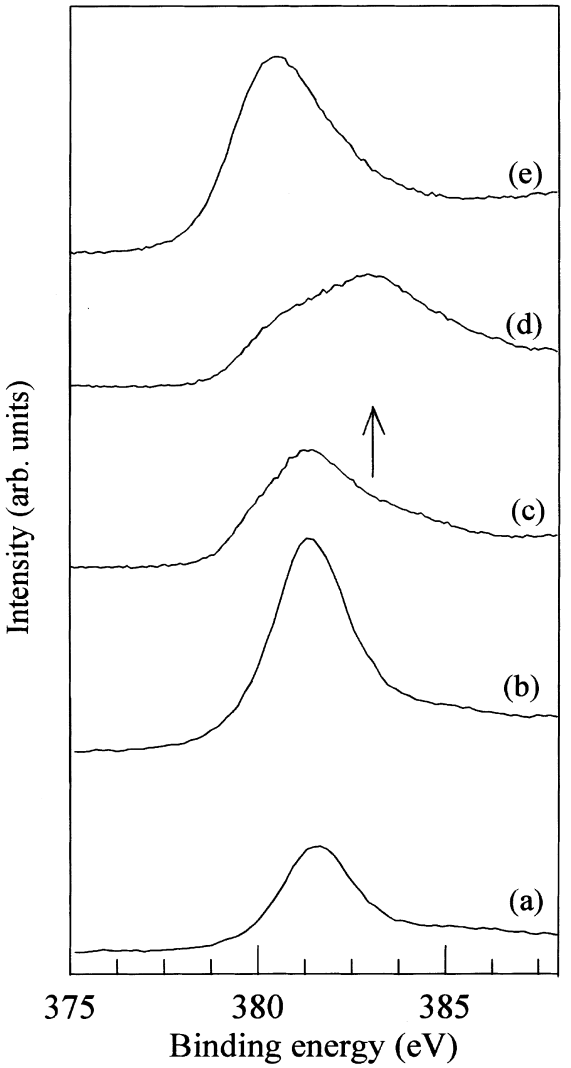

Fig. 9. U($4f_{7/2}$) photoelectric peaks at different stages of decomposition of $UO_2(NO_3) \cdot 6H_2O$: (a) raw sample; (b) stage I residue; (c) stage II residue; (d) stage III residue; and (e) residue after ion beam exposure.

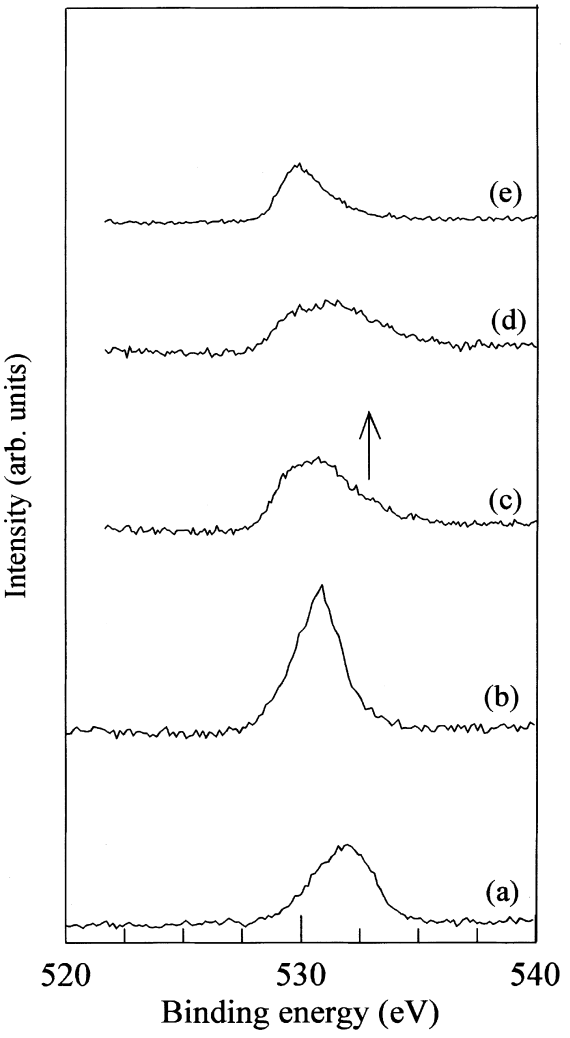

Fig. 10. O(1s) photo electric peaks at different stages of decomposition of $UO_2(NO_3) \cdot 6H_2O$: (a) raw sample; (b) stage I residue; (c) stage II residue; (d) stage III residue; and (e) residue after ion beam exposure.

of UO_2 gives an atomic ratio of 2.1 using the proper sensitivity values of U($4f_{7/2}$) and O(1s) photoelectron peaks). The uranium and oxygen spectra belonging to various decomposition stages are shown in Figs. 9 and 10 respectively. It is known that the U($4f_{7/2}$) photoelectric peak for pure uranium occurs at 377.1 eV and for U^{6+} chemical state, this is observed at 381.7 eV [51]. In our sample $UO_2(NO_3)_2 \cdot 6H_2O$, the binding energy for U($4f_{7/2}$) peak was observed at abnormally higher energy, 387.9 eV, with a characteristic shake up satellite of U^{6+} at 3.9 eV above the main peak. Contaminant C(1s) peak was observed at 290.5 eV which was also high compared to normal contaminant carbon peak at 284.6 eV. Jorgensen et al. has observed the similar binding energy shift in case of $RbUO_2(NO_3)_3$ compound [52] with C(1s) occurring at 290 eV. These unusual shifts can be attributed to surface charging due to photo emission by the insulating material. The corrected values matched well with the literature values [51]. The binding energy values for U($4f_{7/2}$), O(1s) and C(1s) are given in Table 3 after subtraction of charging effects.

Even after the release of water of hydration, NO_x and O_2, the stage I sample did not show any alteration in binding energy of main photo peaks. A reduced oxygen content was inferred from reduction in O(1s) peak area and thereby decreasing the O/U ratio as given in Table 3. The FWHM of O(1s) was observed to reduce from

Table 3
Photoelectric peak positions for $U(4f_{7/2})$, C(1s) and O(1s) at different stages of decomposition of $UO_2(NO_3)_2 \cdot 6H_2O$

Stages	$U(4f_{7/2})$ eV (*Area*)	$U(4f_{5/2})$ characteristics		O(1s eV) (*FWHM*)	C(1s eV)	O/U ratio
		Principal peak eV (*Area*)	Satellite peak eV (*Area*)			
$UO_2(NO_3)_2 \cdot 6\ H_2O$	387.9	398.7	402.6	538.1	290.5	8.0
After charge correction	382.0	392.8 (*32496*)	396.7 (*3228*)	532.2 (*3.2*)	284.6	
Stage I	381.9	392.7 (*66362*)	396.6 (*4181*)	531.2 (*2.6*)	284.6	4.6
Stage II	383.5 (*16047*)	–	–	531.9	284.8	4.0
	381.5 (*51574*)	–	–	530.4		
Stage III	383.5 (*62851*)	–	–	531.8	284.8	3.0
	381.5 (*30471*)	–	–	530.3		
Ion beam exposure	380.8	391.5	398.7	530.3 (*2.3*)	Trace	2.8

3.2 to 2.6 eV after stage I heating to 790 K. In raw sample, O(1s) peak was contributed form O in U–O, N–O and H–O environment and the broad peak was observed due to the convolution of these three peaks. After stage I treatment, the desorption of N–O species dominantly caused drastic decline in the FWHM of the peak. The shake-up satellite observed to be 10% of principal $U(4f_{7/2})$ peak got reduced to 6% indicating a subtle redistribution in valence band. This, as depicted in Fig. 10, is clearly evident from the satellite signature corresponding to $U(4f_{5/2})$ photo emission.

The residue, after stage II O_2 release (950 K), indicated build up of new uranium bearing phases. The dominant peak was observed at 381.5 eV. This represents the +6 oxidation state. A very minor peak at 383.5 eV indicated the onset of formation of new uranium compound. In this compound O(1s) peak upon deconvolution yielded two peaks at 531.9 and 530.4 eV. This signifies two distinct chemical identities i.e. U–O and U–OH bearing phases in the residue. The high binding energy peak due to U–OH bonding is of reduced magnitude and around 24% of the overall U contribution. This indicates U–O bonded compound preponderate over U–O–H bonded one in this residue, which is also seen from XRD data. The C(1s) peak occurs at 284.8 eV indicating absence of charging.

The increase of temperature programme to 1400 K changes the scenario completely. The stage III residue which has been identified from XRD data as a residue compositionally enriched in $UO_3H_{1.17}$ with certain portion of it converted to U_3O_8, also contained an insignificantly minor carry over from stage I residue as evidenced from doubling in the area of uranium peak occurring at 383.3 eV as compared to the area of 381.5 eV peak. The $U(4f_{7/2})$ photo peak of Fig. 9(d) can be construed as a convolution of contributions from compound carried over from stage I residue plus $UO_3H_{1.17}$ and U_3O_8. The O(1s) peak occurs at 531.8 and 530.3 eV. The 531.8 eV peak is the major one signifying renewed co-ordination around oxygen in the lattice. The 530.3 eV can be referred to the signature of carry over compound from stage I [Fig. 10(b)–(d)]. Here again the C(1s) peak occurs at 284.8 eV indicating absence of charging. Table 3 summarises various binding energy values obtained from XPS investigation. Also oxygen to uranium ratios for residues of various stages, deduced from XPS data, are mentioned. This ratio clearly shows a steady rise in heavy metal fraction caused due to progressive loss of oxygen with ascending temperature programme.

The residue left over after stage III treatment was dominated by U–OH type of hydroxilated compound. This residue was exposed to argon ion bombardment inside ESCA machine to see the fate of the material at the extreme case of decomposition i.e. in the eventuality of extending the temperature programme by few hundred degrees more which at the moment is a limitation in our EGA-MS experimental system. At higher temperature one expects complete conversion of the material to thermodynamically stable uranium phase like U_3O_8. An Ar^+ ion beam operating at 3 keV and 1 μA was used for bombardment of the sample inside ESCA machine. After sputtering, the $U(4f_{7/2})$ peak was observed at 380.8 eV with sharp O(1s) peak at 530.3 eV. The binding energy of $U(4f_{7/2})$ indicated the formation of U_3O_8 [51] and sharp O(1s) peak with FWHM 2.3 eV signified the ion bombardment induced dissociation of –OH group from the lattice. The formation of U_3O_8 is further evidenced from $U(4f_{5/2})$ satellite signal occurring around 7.2 eV [52] as seen in Fig. 11.

4. Conclusion

Using EGA-MS, TGA, XRD and XPS, the temperature programmed decomposition of $UO_2(NO_3)_2 \cdot 6H_2O$ has been investigated. Kinetic control regimes for various decomposition stages could be successfully established. Arrhenius parameters like activation energy and pre-exponential factor for various decomposition stages have been calculated. EGA-MS

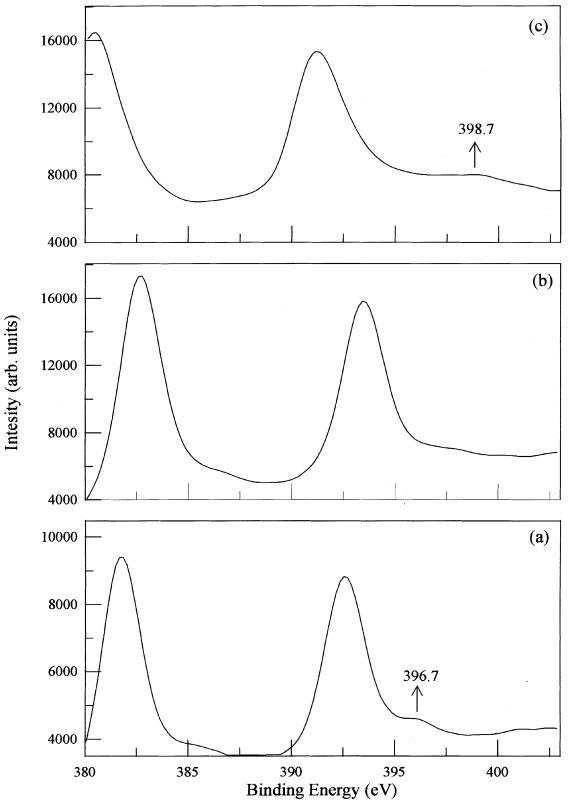

Fig. 11. U($4f_{5/2}$) photoelectric peaks with satellite signal (shown by arrows) at different stages of decomposition: (a) raw $UO_2(NO_3)_2 \cdot 6H_2O$; (b) sample after stage I; and (c) after ion beam exposure.

data could explain complex weight loss profile obtained from TGA. Signature of gas release from various decomposition sequences was found in the concomitant transformation of the residue with respect to substrate crystal structure and uranium chemical environment. It can be emphasised that the pristine uranyl bridge in the lattice of $UO_2(NO_3)_2 \cdot 6H_2O$ was carried forward by temperature programme to the target compound U_3O_8 which also possesses a layered orthorhombic structure with U–O bridge. Progressive shedding of functional units leads to a structural simplification. Also the structural reorganisation of groups leading to formation of $UO_3 \cdot xH_2O$ could be corroborated to valence band shake up inferred from XPS data. However, the present operating temperature range of our EGA-MS system did not permit the substrate to completely transform to thermodynamically stable oxygen bearing uranium phase like U_3O_8. Only a partial transformation was observed. The evidence for the complete conversion of the residue to U_3O_8, possessing a layered orthorhombic lattice with uranium atom having pentagonal bipyramidal co-ordination could be obtained by argon ion bombardment induced dissociation of hydroxilated groups of the final residue. U_3O_8 formation is further corroborated from U($4f_{5/2}$) satellite signal occurring at 7.2 eV.

Acknowledgements

The authors are thankful to G.V.N. Rao and V.S. Shastry for acquiring XRD patterns, Dr V. Sridharan for TGA runs and Dr B. Purniah and J. Jayapandian for instrumentation support. The authors are grateful to Dr P. Rodriguez, Director, IGCAR, Kalpakkam for his encouragement and support to this activity.

References

[1] D.O. Campbell, in: Light Water Nuclear Reactor Fuel Cycle, R.G. Wymer, B.L. Vondra Jr. (Eds.), CRC, FL, 1981.
[2] R.E. Lerch, R.E. Norman, Radiochim. Acta 36 (1984) 75.
[3] P.A. Haas, Nucl. Techol. 81 (1988) 393.
[4] D. Warin, A. Caillol, A. Gabriac, IAEA Technical Committee on Recycling of Plutonium and Uranium in Water Reactor Fuels, Cuduroche, France, 13–16 November 1989.
[5] M. Koizumi, K. Ohtsuka, H. Isagawa, H. Akiyama, A. Todokoro, Nucl. Techol. 61 (1983) 55.
[6] H. Oshima, J. Nucl. Sci. Technol. 26 (1) (1989) 161.
[7] Szekely, in: P. Barrot, L.C. Dufour, Materials Science Monographs, 28A, Part A, Elsevier, Amsderdam, 1985.
[8] J.E. Fleming, H. Lynton, Chem. Ind. 19 (1960) 1416.
[9] J.C. Taylor, M.H. Muller, Acta Crystallogr. 19 (1965) 536.
[10] B.M. Gatehouse, A.E. Comyns, J. Chem. Soc., part IV (1958) 3965.
[11] J.L. Woodhead, A.M. Deane, A.C. Fox, J.M. Fletcher, J. Inorg. Nucl. Chem. 28 (1966) 2175.
[12] R.S. Ondrejcin, T.P. Garrett Jr., J. Phys. Chem. 65 (1961) 470.
[13] W. Lodding, L. Ojama, J. Inorg. Nucl. Chem. 27 (1965) 1267.
[14] K.V. Rajagopalan, P.V. Ravindran, T.P. Radhakrishnan, J. Thermal Anal. 44 (1995) 89.
[15] M.L. Franklin, T.B. Flanagan, J. Chem. Soc. Dalton Transactions 1 (1972) 192.
[16] W.H. Smith, J. Inorg. Nucl. Chem. 30 (1968) 1761.
[17] P.T. Moseley, C.J. Seabrook, J. Chemical Society Dalton transactions 10 (1973) 1115.
[18] F. Weigel, in: J.J. Katz, G.T. Seaborg, L.R. Morss (Eds.), Chemistry of the Actinide Elements, ed. 2, vol. 1, Chapman and Hall, London, 1986.
[19] P.K. Gallgher, Thermochim. Acta 26 (1978) 175.
[20] P.K. Gallagher, J. Thermal Anal. 25 (1982) 7.
[21] H.G. Langer, in: E.J. Elving (Ed.), Treatise on Analytical Chemistry, Part 1, 2nd ed., vol. 12, Wiley, New York, 1983.
[22] W.W. Wendlandt, Thermal Analysis, 3rd ed., Wiley, New York, 1986.
[23] D. Price, D. Dollimore, N.S. Fatemi, R. Whitehead, Thermochim. Acta 42 (1980) 323.

[24] D. Price, N.S. Fatemi, D. Dollimore, R. Whitehead, Thermochim. Acta 94 (1985) 313.
[25] A.W. Coats, J.P. Redfern, Nature 201 (1964) 68.
[26] E.S. Freeman, B. Carroll, J. Phys. Chem. 62 (1958) 394.
[27] A.M. Gadalla, Thermochim. Acta 95 (1985) 179.
[28] M.E. Brown, D. Dollimore, A.K. Galwey, in: Bamford, C.F.H. Tipper (Eds.), Comprehensive Chemical Kinetics, vol. 22, Reactions in the Solid State, Amsterdam, Elsevier, 1980.
[29] M. Kamruddin, P.K. Ajikumar, S. Dash, B. Purniah, A.K. Tyagi, K. Krishan, Instrument. Sci. Technol. 23 (2) (1995) 123.
[30] S. Dash, M. Kamruddin, P.K. Ajikumar, A.K. Tyagi, K. Krishan, Bull. Ind. Vacuum Soc. 26 (4) (1995) 31.
[31] J. Sestak, V. Satava, W.W. Wendlandt, Thermochim. Acta 7 (1973) 332.
[32] M.E. Brown, Introduction to Thermal Analysis, Chapman and Hall, London, 1988.
[33] M. Kamruddin, P.K. Ajikumar, S. Dash, R. Krisnan, A.K. Tyagi, K. Krishan, J. Thermal Anal. 48 (1997) 277.
[34] B. Jezowska - Trzebiatowska, B. Kedzia, Bull. Acad. Polan. Sci. Ses. Sci. Chim. 12 (1964) 251.
[35] J. Szekely, J.W. Evans, H.Y. Sohn, Gas Solid Reactions, Academic Press, New York, 1976.
[36] N. Kent Dalley, M.H. Mueller, S.H. Simonsen, Inorg. Chem. 10 (2) (1971) 323.
[37] H. Tanaka, N. Koga, A.K. Galway, J. Chem. Educ. 72 (3) (1995) 251.
[38] M. Kamruddin, P.K. Ajikumar, S. Dash, R. Krishnan, A.K. Tyagi, K. Krishan, Thermochim. Acta 287 (1996) 13.
[39] M. Baber, G. Schumacher, in: E.J. Henley, J. Lewins, Advances in Nuclear Science and Technology, vol. 7, Academic Press, New York, 1973.
[40] F.A. Nichols, J. Nucl. Mater. 84 (1979) 1.
[41] M. C Ball, C.R.G. Birkett, D.S. Brown, M.J. Jaycock, J. Inorg. Nucl. Chem. 36 (1974) 1577.
[42] A.M. Deane, J. Inorg. Nucl. Chem. 21 (1961) 238.
[43] M.J. Bannister, J.C. Taylor, Acta Crystallogr. B 26 (1970) 1775.
[44] J.C. Taylor, Acta Crystallogr B 27 (1971) 1088.
[45] J.C. Taylor, H.J. Hurst, Acta Crystallogr. B 27 (1971) 2018.
[46] S. Siegel, H.R. Hoekstra, E. Gebert, Acta Crystallogr. B 28 (1972) 3469.
[47] P.G. Dickens, S.B. Hawke, M.T. Weller, Mater Res. Bull. 19 (1984) 543.
[48] W. Lodding, L. Ojama, J. Inorg. Nucl. Chem. 27 (1968) 1745.
[49] B.O. Loopstra, Acta Crystallogr. 17 (1964) 651.
[50] S. Bera, S.K. Sali, S. Sampath, S.V. Narasimhan, V. Venugopal, J. Nucl. Mater. 255 (1998) 26.
[51] D. Chadwick, Chem. Phys. Letts. 21 (1973) 291.
[52] J.J. Pireaux, J. Riga, E. Thibaut, C. Tenret-noel, R. Caudano, J.J. Verbist, Chem. Phys. 22 (1977) 113.